

A 63 *m* Superconcentrated Aqueous Electrolyte for High-Energy Li-Ion Batteries

Long Chen,[▽] Jiaxun Zhang,[▽] Qin Li,[▽] Jenel Vatamanu, Xiao Ji, Travis P. Pollard, Chunyu Cui, Singyuk Hou, Ji Chen, Chongyin Yang, Lin Ma, Michael S. Ding, Mounesha Garaga, Steve Greenbaum, Hung-Sui Lee, Oleg Borodin,* Kang Xu,* and Chunsheng Wang*

Cite This: *ACS Energy Lett.* 2020, 5, 968–974

Read Online

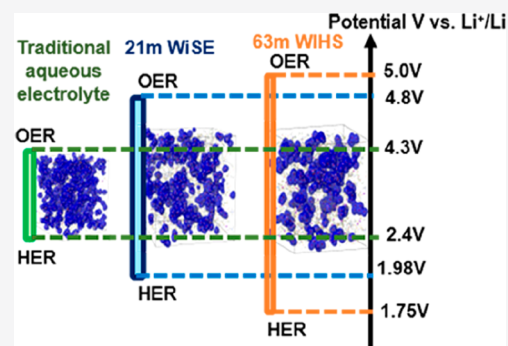
ACCESS |

Metrics & More

Article Recommendations

Supporting Information

ABSTRACT: A water-in-salt electrolyte (WiSE) offers an electrochemical stability window much wider than typical aqueous electrolytes but still falls short in accommodating high-energy anode materials, mainly because of the enrichment of water molecules in the primary solvation sheath of Li⁺. Herein, we report a new strategy in which a non-Li cosalt was introduced to alter the Li⁺-solvation sheath structure. The presence of an asymmetric ammonium salt (Me₃EtN⁺TFSI) in water increases the solubility of LiTFSI by two times, pushes the salt/water molar ratio from 0.37 in WiSE to an unprecedented value of 1.13, and significantly suppresses the water activity in both bulk electrolyte and the Li⁺-solvation sheath. This new 63 *m* (mol kg_{solvent}⁻¹) aqueous electrolyte (42 *m* LiTFSI + 21 *m* Me₃EtN⁺TFSI) offers a wide potential window of 3.25 V and supports a 2.5 V aqueous Li-ion battery (LiMn₂O₄/Li₄Ti₅O₁₂) to deliver a high energy density of 145 Wh kg⁻¹ stably over 150 cycles.



The public concern over the safety of lithium ion batteries (LIB) increases rapidly with our reliance on this technology in our daily life,^{1–4} for which the nonaqueous and highly flammable electrolyte should bear most of the responsibility. Aqueous batteries offer a safe alternative;^{5–7} however, the narrow electrochemical stability window of a typical aqueous electrolyte (<2.0 V) imposed by the electrolysis of H₂O (hydrogen evolution reaction (HER) at anode and oxygen evolution reaction (OER) at cathode) sets a crippling limit on the energy density of all aqueous batteries. To break this confinement, the scientific solution is to reduce the electrochemical activity of water molecules in a Li⁺-solvation sheath as well as in the bulk electrolyte.

Recently, a new class of aqueous electrolytes, “water-in-salt electrolyte” (WiSE), was developed by dissolving a tremendous amount of Li salt in water, pushing the salt/water molar ratio from 0.018 (corresponding to typical 1.0 *m* (mol kg_{solvent}⁻¹) diluted electrolytes) to 0.37–0.50 (corresponding to 21 *m* WiSE or 28 *m* water-in-bisalt (WiBS)), exhibiting an electrochemical stability window of ~3.0 V.^{8–14} At these high-concentrations, because the average number of water molecules available to solvate each Li⁺ falls far below the “solvation numbers” required to establish a normal Li⁺-solvation sheath, significant change occurs to both the Li⁺-solvation sheath structure as well as the bulk electrolyte liquid structure, which results in an altered interfacial chemistry on

both electrode surfaces.⁹ However, further increasing Li salt concentration beyond 28 *m* is often limited by salt solubility and results in high viscosity and poor ion conduction. Very recently, Hu et al. introduced tetraethylammonium into an aqueous electrolyte for a sodium ion battery, which helps to increase the salt concentration to 31 *m*.¹⁵ The highest concentration achieved thus far of 55.6 *m* was enabled by an asymmetric derivative of TFSI anion, pushing the salt/water molar ratio to 1.0. However, its viscosity significantly increased to 8555 mPa s and is accompanied by a decrease in ion conductivity (~0.1 mS cm⁻¹),¹⁶ indicating that such approaches quickly becomes unsustainable if water activity needs to be further reduced.

Herein, we report an alternative approach. Using an inert salt based on an asymmetric ammonium cation, trimethylammonium (Me₃EtN⁺), the solubility of LiTFSI can be increased by two times. The resultant new class of water-in-hybrid-salt (WIHS) aqueous electrolyte contains an unprece-

Received: February 15, 2020

Accepted: February 27, 2020

Published: February 27, 2020

Table 1. Physicochemical Properties of WIHS Electrolytes

material	salt molality (mol kg ⁻¹)	viscosity (mPa s)	glass temperature θ_g (°C)	liquidus temperature θ_l (°C)	solidus temperature θ_s (°C)	conductivity ^a (mS cm ⁻¹)
WIHS electrolyte	63	407	-66.1	23.4	-17.6	0.91

^aViscosity and ionic conductivity were measured at room temperature.

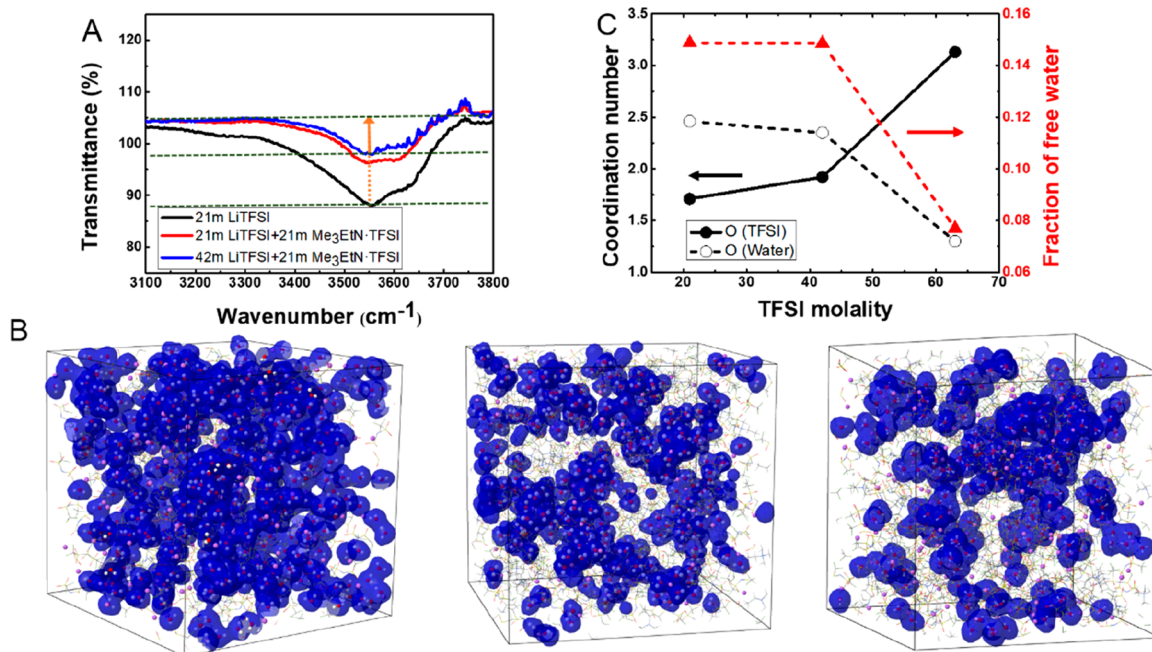


Figure 1. FTIR and MD simulation results of liquid structure. (A) FTIR spectra of 21 *m* WiSE (21 *m* LiTFSI), 42 *m* WIHS (21 *m* LiTFSI + 21 *m* Me₃EtN·TFSI), and 63 *m* WIHS (42 *m* LiTFSI + 21 *m* Me₃EtN·TFSI) electrolytes. (B) Snapshots of MD simulation box showing connectivity of the Li⁺(H₂O) chains (domain) highlighted with transparent blue for 21 *m* WiSE (21 *m* LiTFSI), 42 *m* WIHS (21 *m* LiTFSI + 21 *m* Me₃EtN·TFSI), and 63 *m* WIHS (42 *m* LiTFSI + 21 *m* 3MeEtN·TFSI) electrolytes (from left to right). The TFSI⁻ anions and Me₃EtN⁺ anions are shown as wireframe. Colors: Li, purple; O, red; H, white. (C) Coordination numbers of O(TFSI) and O(water) around Li⁺ (within 2.8 Å) and a fraction of free water (no Li⁺ within 2.8 Å) for 21 *m* WiSE (21 *m* LiTFSI), 42 *m* WIHS (21 *m* LiTFSI + 21 *m* Me₃EtN·TFSI), and 63 *m* WIHS (42 *m* LiTFSI + 21 *m* 3MeEtN·TFSI) electrolytes.

dedented high salt concentration of 63 *m* (42 *m* LiTFSI + 21 *m* Me₃EtN·TFSI), pushing the salt/water molar ratio to 1.13 for the very first time. Despite the high salt concentration, the 63 *m* WIHS maintains a relatively high ionic conductivity of 0.91 mS cm⁻¹ and low viscosity of 407 mPa s, while demonstrating a wide electrochemical stability window of 3.25 V (1.75 V cathodic and 5.0 V anodic vs Li⁺/Li). The electrolyte supports a 2.5 V aqueous LIB (LiMn₂O₄//Li₄Ti₅O₁₂) full cell to deliver a high energy density of 145 Wh kg⁻¹ over 150 cycles at 1 and 0.2 C. Beyond their application for high energy storage technologies, the hybrid-salt approach presents a new class of superconcentrated electrolytes, whose unexplored bulk ion transport, liquid structure, interfacial structure, and interphasial chemistries at electrodes provide exciting scientific opportunities for physical chemistry and electrochemistry.

At room temperature, the maximum solubility of neat LiTFSI in H₂O is ~22 *m*, above which salt inevitably precipitates. The LiTFSI salt solubility could be doubled when the asymmetric ammonium salt (Me₃EtN·TFSI) is present, resulting in a maximum concentration of 63 *m* (42 *m* LiTFSI + 21 *m* Me₃EtN·TFSI, Figure S1). Interestingly, Me₃EtN·TFSI alone cannot dissolve in water (Figure S2). Hence, the formulation of WIHS electrolytes requires the simultaneous presence of both LiTFSI and Me₃EtN·TFSI, a phenomenon that hints at an unusual liquid structure.

Table 1 summarizes some important physicochemical properties of the 63 *m* WIHS electrolyte, of which the thermal properties were characterized using differential scanning calorimetry (DSC). Thermodynamically, this electrolyte is a stable liquid with its liquidus temperature θ_l of 23.4 °C below ambient temperature and consists of solid phases only when below its solidus temperature θ_s of -17.6 °C (Figure S3). Kinetically, however, it proved to be highly resistant to crystallization, as evidenced by the complete lack of crystallization events during the first cooling of its DSC sample down through its glass transition below -60 °C at -5 °C min⁻¹ (Figure S3), which enabled its glass temperature θ_g (-66 °C) to be determined in subsequent heating. The glass transition was not followed by crystallization as usual; only on the second heating through its θ_g did crystallization finally occur. This strong resistance to crystallization makes the electrolyte a good candidate for low-temperature use. The value of θ_s here should be equal to that of the eutectic temperature of the ternary Li(H₂O)₄·TFSI-LiH₂O·TFSI-Me₃EtN·TFSI, as the composition of 42 *m* LiTFSI lies between the two solid LiTFSI hydrates as identified in ref 17. It is further assumed that Me₃EtN·TFSI does not form stable hydrates because of the large size of and the diffused electric charge on the cation, which has been confirmed by the very limited solubility (Figure S2). Here, although the salt

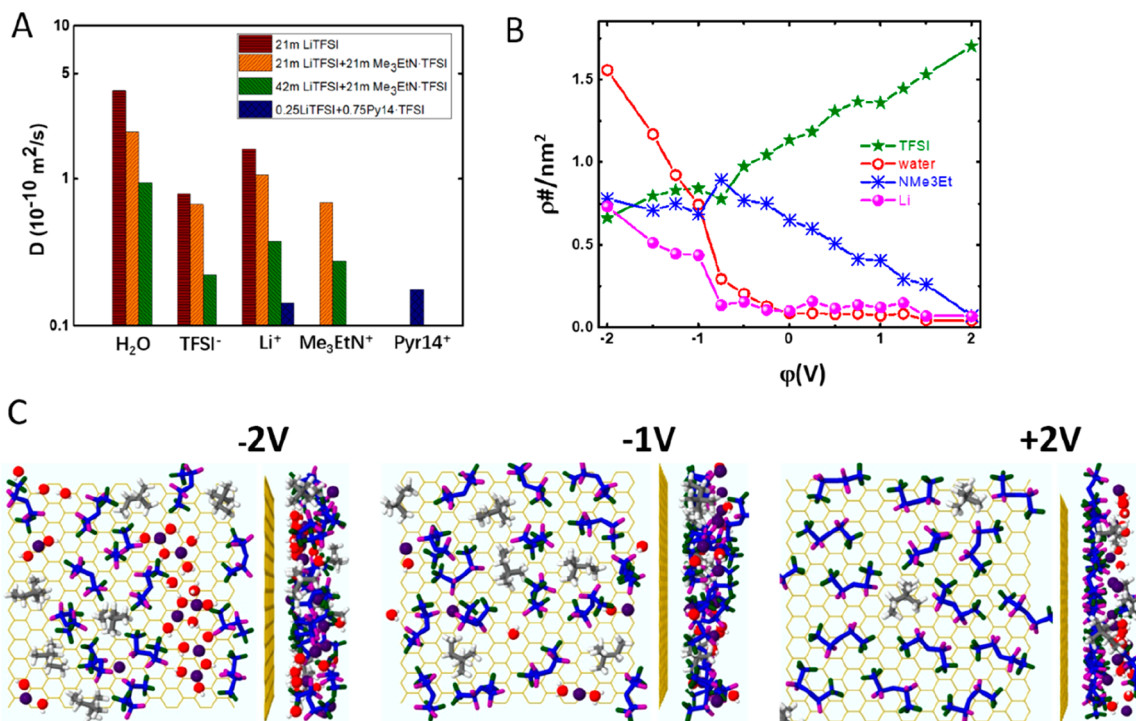


Figure 2. MD simulation results of self diffusion and double layer. (A) Self-diffusion coefficients for 21 *m* WiSE (21 *m* LiTFSI), 42 *m* WIHS (21 *m* LiTFSI + 21 *m* Me₃EtN·TFSI), and 63 *m* WIHS (42 *m* LiTFSI + 21 *m* Me₃EtN·TFSI) electrolytes and nonaqueous neat RTIL electrolyte (0.25LiTFSI + 0.75Pyr₁₄·TFSI) at 333 K. (B) Interfacial composition of the inner part of the double layer of 63 *m* WIHS electrolyte on graphite showing number density. (C) Snapshots of the inner part of the double layer of 63 *m* WIHS (top and side views for three potentials relative to potential of zero charge).

concentration approaches an astonishing value of 63 *m*, the viscosity remains relatively low (407 mPa s, in sharp comparison with 8555 mPa s of a 55.56 *m* neat Li salt electrolyte),¹⁶ and it retains an ionic conductivity of 0.91 mS cm⁻¹, which is close to the minimum value required to support acceptable battery operations.

The interplay among Li⁺, Me₃EtN⁺, TFSI⁻, and water was evaluated using Fourier transform infrared (FTIR) spectroscopy. The bands in the FTIR spectra at ~3550 cm⁻¹ and ~3650 cm⁻¹ (Figure 1A) are attributed to O–H stretching in H₂O,^{18,19} and the intensity of these two peaks decreases significantly in the 63 *m* WIHS electrolyte as compared to that of 21 *m* WiSE. Compared to pure water, the FTIR spectrum reveals that the hydrogen bonding network is severely disrupted.^{20,21}

Molecular dynamics (MD) simulations were performed on both 42 *m* WIHS (21 *m* LiTFSI + 21 *m* Me₃EtN·TFSI) and 63 *m* WIHS (42 *m* LiTFSI + 21 *m* Me₃EtN·TFSI), and their structural and dynamics properties were compared with 21 *m* WiSE. Radial distribution functions (RDFs) shown in Figure S4 reveal that Li⁺ prefers to coordinate with oxygen of water (O_w) rather than oxygen of TFSI⁻ (O_{TFSI}). The strong Li–water affinity leads to a rather high fraction of the solvent separated ion pairs (SSIP) Li⁺(H₂O)TFSI and high fraction of Li⁺(H₂O)₄ complexes as shown in Figure S5a. The SSIP is approximately the same for 21 *m* WiSE and 42 *m* WIHS, but further addition of 21 *m* of LiTFSI decreases the fraction of the SSIP Li⁺(H₂O)₄ complexes by a factor of 2, thus reducing the number of charge carriers in the 63 *m* WIHS electrolyte. A spatial distribution of the Li⁺(H₂O)₄ solvates in the MD simulation boxes is shown in Figure 1B, while the distribution of the O_w–O_w cluster sizes is shown in Figure S5b. In 21 *m*

WiSE, a significant fraction of the O_w–O_w networks percolates through the entire MD simulation box. Adding 21 *m* Me₃EtN·TFSI decreases the size of the [Li⁺(H₂O)₄]_n clusters with the most probable size being around 10–30 water molecules. Further addition of 21 *m* LiTFSI to 42 *m* WIHS results in the further breakdown of water domains (clusters) with the most probable cluster size becoming even smaller. In 63 *m* WIHS electrolyte rearrangement of the Li⁺(H₂O)₄ clusters is necessary for Li⁺ transport through the water-rich phase. The Li⁺ transport also occurs through the anion-rich domain that contains 25% Li⁺ for 42 *m* WIHS and 50% for 63 *m* WIHS electrolyte. These domains are water-poor and are composed of the (TFSI–Li–TFSI) networks. As shown before, Li⁺ diffusion through the TFSI-rich domain is much slower compared to the diffusion through the Li⁺(H₂O)₄-rich domain.²²

Figure 1C shows that addition of 21 *m* Me₃EtN·TFSI to 21 *m* WiSE does not change the structure of the primary Li⁺-solvation sheath, while further addition of 21 *m* LiTFSI increases the number of O_{TFSI} at the expense of the number of water in the Li⁺-solvation sheath. Importantly, the fraction of free water that is not coordinated by a Li⁺ decreases by a factor of 2 in 63 *m* WIHS as compared to 21 *m* WiSE and 42 *m* WIHS. In 63 *m* WIHS, each TFSI⁻ is surrounded by 1.74 Li⁺ on average with the Li–TFSI–Li coordination being the most favorable (Figure S5c). Higher number of Li⁺ near TFSI⁻ stabilizes an excess electron, increases electrolyte reduction potential, and destabilizes the excess hole, leading to higher oxidation potential.^{9,23} Together with the reduced water presence in Li⁺-solvation sheath as well as the decreased fraction of free water in bulk 63 *m* WIHS electrolyte, these changes of the TFSI⁻ coordination would likely favor a more

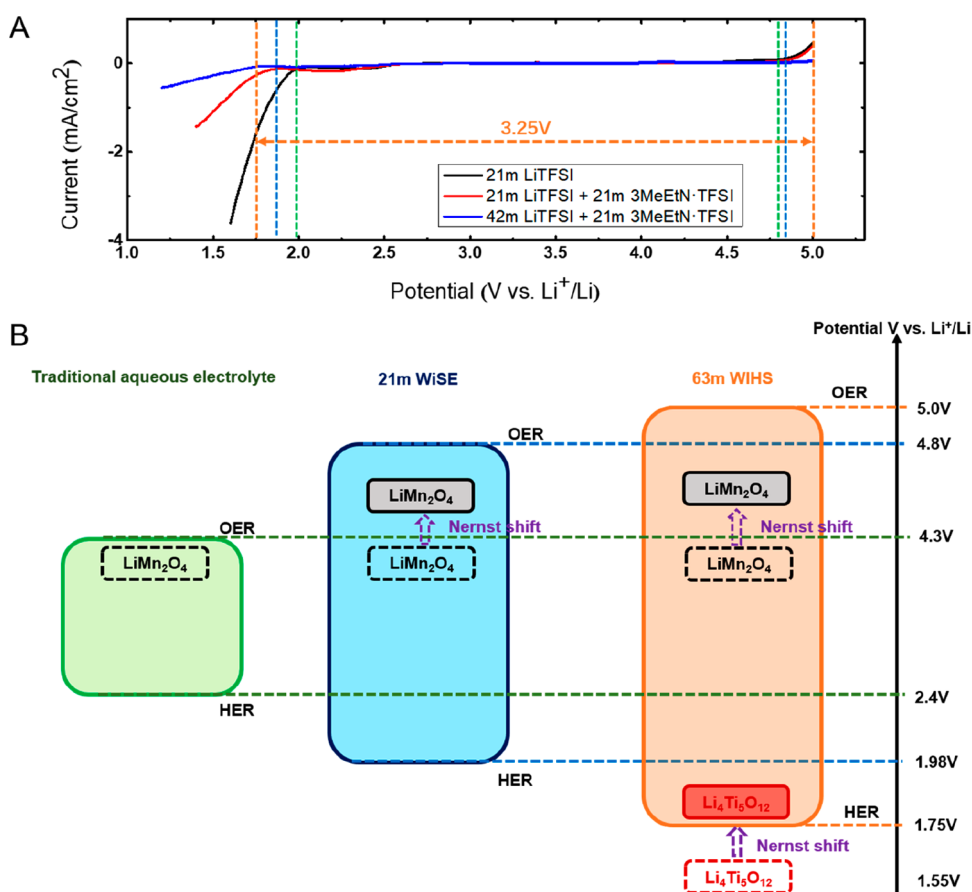


Figure 3. Electrochemical window of WIHS electrolyte. (A) Electrochemical windows of different aqueous electrolytes as measured on inactive current collector (stainless steel) at scanning rate of 5 mV s^{-1} . (B) Illustration of expanded electrochemical stability window for 63 *m* (42 *m* LiTFSI + 21 *m* Me₃EtN·TFSI) WIHS electrolyte together with the modulated redox couples of LiMn₂O₄ cathode and Li₄Ti₅O₁₂ anode caused by high salt concentration.

exclusive TFSI[−] reduction over H₂ and O₂ evolution, thus extending the electrochemical stability window.

The diffusivities of ⁷Li, ¹H, and ¹⁹F were predicted from MD simulations and also measured separately by PFG-NMR, which correspond to the movements of Li⁺, ammonium and water, and anion (TFSI[−]), respectively. Table S1 shows that the apparent transference numbers of Li⁺ (*t*_{Li⁺}) in 42 *m* WIHS and 63 *m* WIHS as measured by NMR are 0.38 and 0.51, respectively. These lower transference numbers as compared with that of WiSE (0.71) actually does not mean that Li⁺ moves slower than TFSI[−], but rather originates from the fact that Li⁺ now is no longer the only cationic carrier but has a competitor. Nevertheless, Li⁺ remains the most mobile ionic species for 63 *m* WIHS. There is excellent agreement between these transference numbers and those calculated via MD simulations (0.386 for 42 *m* WIHS and 0.505 for 63 *m* WIHS). Such excellent agreement between the experimental values and predictions further validates the reliability of the force field in describing ion and solvent transport in this complex system.

A comparison of self-diffusion coefficients among 21 *m* WiSE, 42 *m* WIHS, 63 *m* WIHS electrolytes, and neat room-temperature ionic liquid (RTIL) (LiTFSI-Pyr₁₄·TFSI) electrolyte (Pyr₁₄ stands for methylbutyl pyrrolidinium, a heteroatomic version of ammonium cation) is given in Figure 2A. Addition of Me₃EtN·TFSI into 21 *m* WiSE only slightly slows down the movement of TFSI[−], water, and Li⁺, while further addition of another 21 *m* of LiTFSI had a more dramatic effect

on all the diffusion coefficients. In the 63 *m* WIHS electrolyte, Li⁺ diffuses significantly faster than that in the neat RTIL electrolyte (0.25LiTFSI + 0.75Pyr₁₄·TFSI). Thus, the Li⁺ conductivity is much higher in the 63 *m* WIHS than that in the neat RTIL electrolyte, suggesting that this electrolyte, despite its high salt concentration, is expected to support higher rate cycling in batteries. In 21 *m* WiSE, 42 *m* WIHS, and 63 *m* WIHS electrolytes, the Li⁺ cation is the fastest moving ionic species in contrast to the neat nonaqueous RTIL electrolyte, where Li⁺ is the slowest moving species. Therefore, in WiSE and WIHS electrolytes, *t*_{Li⁺} is expected to be higher than that in the neat RTIL electrolyte. Furthermore, the transport mechanism significantly differ between the WIHS and the neat RTIL electrolytes. In RTIL the migration of Li⁺(TFSI[−])_{*n*} requires counter diffusion of the free TFSI[−] anions.²⁴ In the aqueous WIHS, however, the vehicular motion of much lighter Li⁺(H₂O)_{*n*} is expected to dominate the cation transport, leading to higher *t*_{Li⁺}. This is consistent with the experimental results by PFG-NMR tests (Table S1); the *t*_{Li⁺} in 63 *m* WIHS electrolyte is 0.51, which is much higher than that of 0.099 in neat RTIL. The ionic conductivities of 63 *m* WIHS and neat RTIL electrolytes are compared in Table S2, with 0.91 mS cm^{−1} for the former and 0.45 mS cm^{−1} for the latter. To make the comparison on a fairer basis, we also prepared another 63 *m* WIHS (42 *m* LiTFSI + 21 *m* Pyr₁₄·TFSI), in which the *t*_{Li⁺} and ionic conductivity are 0.46 and 0.86 mS cm^{−1}, respectively (Table S2), both being much

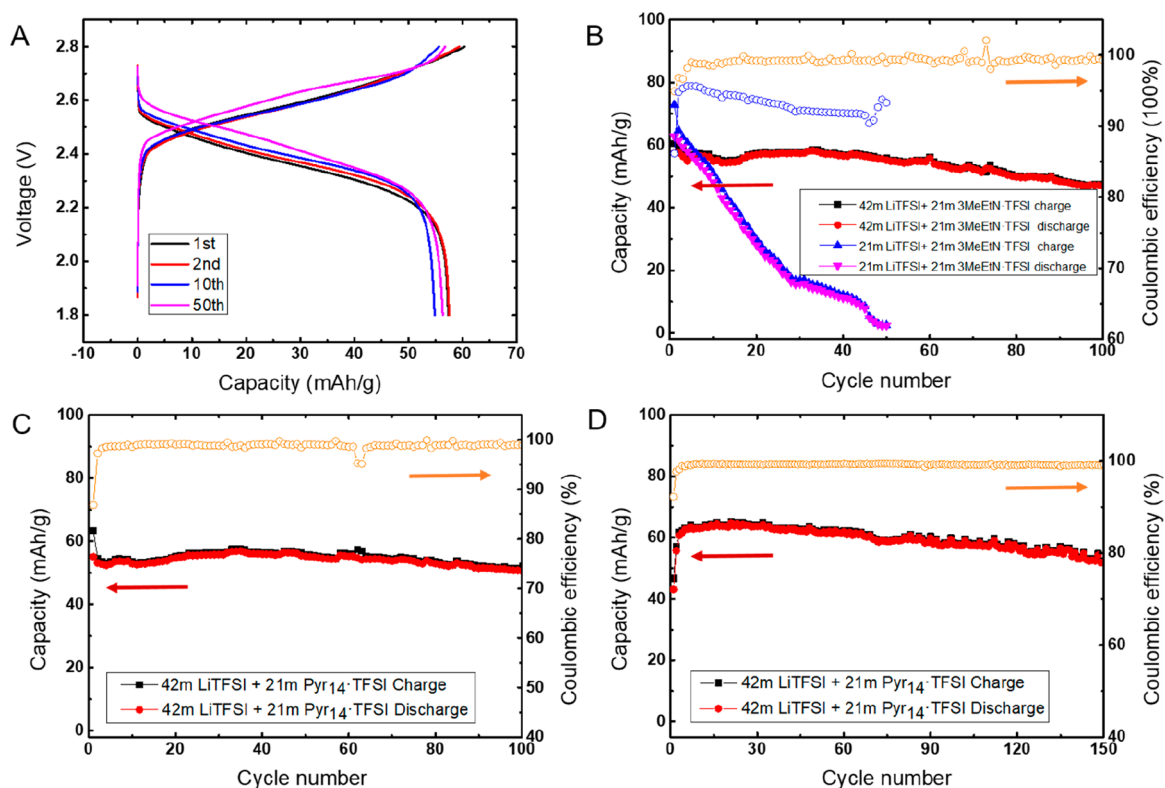


Figure 4. High-energy aqueous Li-ion batteries. (A) Selected charge–discharge voltage profiles of $\text{LiMn}_2\text{O}_4//\text{Li}_4\text{Ti}_5\text{O}_{12}$ full cell with the 63 *m* WIHS aqueous electrolyte (42 *m* LiTFSI + 21 *m* $\text{Me}_3\text{EtN}\cdot\text{TFSI}$) at the rate of 1 C. (B) Cycling stability and Coulombic efficiency of $\text{LiMn}_2\text{O}_4//\text{Li}_4\text{Ti}_5\text{O}_{12}$ full cell with the 63 *m* WIHS aqueous electrolyte (42 *m* LiTFSI + 21 *m* $\text{Me}_3\text{EtN}\cdot\text{TFSI}$) at the rate of 1 C. (C) Cycling stability and Coulombic efficiency of $\text{LiMn}_2\text{O}_4//\text{Li}_4\text{Ti}_5\text{O}_{12}$ full cell with the 63 *m* WIHS aqueous electrolyte (42 *m* LiTFSI + 21 *m* $\text{Pyr}_{14}\cdot\text{TFSI}$) at the rate of 1 C. (D) Cycling stability and Coulombic efficiency of $\text{LiMn}_2\text{O}_4//\text{passivated-Li}_4\text{Ti}_5\text{O}_{12}$ full cell with the 63 *m* WIHS aqueous gel electrolyte (42 *m* LiTFSI + 21 *m* $\text{Pyr}_{14}\cdot\text{TFSI}$) at the rate of 0.2 C. All the specific capacity values are calculated based on the total mass of cathode and anode.

higher than that of neat RTIL electrolyte (0.25LiTFSI + 0.75 $\text{Pyr}_{14}\cdot\text{TFSI}$). In addition, for the neat RTIL electrolyte system, it is difficult to reach such a high Li^+/RTIL ratio of 2 without water, which significantly limited its Li^+ conductivity.

The electrical double layer (EDL) structure is closely coupled with interfacial electrochemistry. We investigated the influence of potential on the electrolyte interfacial structure using a graphite electrode as an initial model system as shown in Figure S6 and described in detail in the Supporting Information. MD simulations show that anions strongly partition to the positive electrode surface pushing water away from the interface, thus screening the water–electrode interactions as shown in Figures 2B–C and S7. This mechanism is partly responsible for the extension of electrolyte anodic stability together with the reduction of the fraction of free water present in electrolyte with increasing salt concentration from 21 to 63 *m*.²⁵ At potentials above -0.8 V vs potential of zero charge (PZC) little water is accumulated at the electrode surface as the inner part of the EDL is dominated by the TFSI^- anions and MeEt_3N^+ cations.²³ Even at potentials below -1 V vs PZC when Li^+ approaches the electrode surface and brings water with it, there is significantly less (by a factor of 2) water in the inner part of EDL compared to 28 *m* WiBS (21 *m* LiTFSI + 7 *m* LiOTF) electrolyte.²⁵ The Me_3EtN^+ competes with the $\text{Li}^+(\text{H}_2\text{O})_n$ solvates at the interfacial layer and assists in pushing water away from the interface. Importantly, because of high LiTFSI salt concentration in 63 *m* WIHS electrolyte, each TFSI^- anion is

coordinated by two Li^+ on average at the negatively polarized electrode (see Figure S8). A higher number of Li^+ near TFSI^- is expected to stabilize the excess electrons on the TFSI^- during reduction, increase salt reduction potential, and facilitate salt decomposition at higher potentials minimizing hydrogen evolution from water.^{9,23}

The electrochemical stability windows of 21 *m* WiSE, 42 *m* WIHS, and 63 *m* WIHS aqueous electrolytes were evaluated using linear sweep voltammograms on nonactive stainless-steel electrodes (Figure 3A). The potential for hydrogen evolution, which sets the cathodic limit for the electrochemical stability window, was negatively shifted from 1.98 V in 21 *m* WiSE to 1.85 V in 42 *m* WIHS, and further to 1.75 V in 63 *m* WIHS electrolyte. The cathodic current at 1.6 V was also significantly diminished from 3.62 mA cm^{-2} in 21 *m* WiSE to 0.2 mA cm^{-2} in 63 *m* WIHS, demonstrating that the reductive decomposition of water is significantly suppressed because of the solvation sheath structure change in the 63 *m* WIHS, where each Li^+ sees the replacement of water molecules by TFSI^- when salt concentration increases to 63 *m*. Such a solvation sheath structure promotes the formation of a robust interphase that inhibits water reduction. On the cathode side, 63 *m* WIHS also extends the anodic limit from 4.9 V in 21 *m* WiSE to 5.0 V, because in WIHS the higher concentration of TFSI^- also results in a better screening of $\text{Li}^+(\text{H}_2\text{O})_n$ from the positively charged electrode as shown in Figure 2B,C.²³ Over all, an electrochemical stability window of ~ 3.25 V (1.75–5.0 V vs Li^+/Li) is achieved in this 63 *m* WIHS aqueous electrolyte.

Because of the extra high salt concentration, the redox reaction potentials of all electrodes are shifted upward by approximately 0.3 V as predicted by the Nernst equation (Figure 3B). This concentration effect thus moves the operation potential of $\text{Li}_4\text{Ti}_5\text{O}_{12}$ into the 1.75–5.0 V electrochemical stability window and enables a full Li^+ intercalation–deintercalation reaction of this anode material, which has been challenging for all aqueous electrolytes because of the strong catalyzing nature of titanates to split water.

The electrochemical behavior of the 63 *m* WIHS aqueous electrolyte was verified in a full Li-ion cell using a LiMn_2O_4 cathode and $\text{Li}_4\text{Ti}_5\text{O}_{12}$ anode. The cathode/anode capacity ratio is adjusted to be 1.1:1 to compensate the irreversible capacity associated with the solid electrolyte interphase (SEI) formation on the $\text{Li}_4\text{Ti}_5\text{O}_{12}$ anode during the initial few cycles. The discharge profile displayed a slope from 2.6 to 2.3 V, delivering a discharge capacity of 56 mAh g^{-1} (calculated based on the total mass of LiMn_2O_4 cathode and $\text{Li}_4\text{Ti}_5\text{O}_{12}$ anode) at the rate of 1 C (Figure 4A). A conservatively estimated energy density of a $\text{LiMn}_2\text{O}_4/\text{Li}_4\text{Ti}_5\text{O}_{12}$ full cell from the average voltage and capacity is 145 Wh kg^{-1} (of total electrode mass). Surprisingly, the initial Coulombic efficiency of the $\text{LiMn}_2\text{O}_4/\text{Li}_4\text{Ti}_5\text{O}_{12}$ full cell is as high as 95%, which quickly increases to 99.5% within 10 cycles. A high capacity retention of 88% is maintained after 100 cycles at 1 C (Figure 4B), outperforming the $\text{LiMn}_2\text{O}_4/\text{Li}_4\text{Ti}_5\text{O}_{12}$ full cell in 42 *m* WIHS electrolyte. The chemical composition of the formed SEI was identified to be mainly LiF by X-ray photoelectron spectroscopy (XPS), which was performed on $\text{Li}_4\text{Ti}_5\text{O}_{12}$ anode recovered from the cycled full Li-ion cell. The conspicuous F 1s signal at 684.67 eV indicated a dense and strong SEI (Figure S9).

We also evaluated the alternative aqueous electrolyte, wherein the inert cation is pyrrolidinium. The $\text{LiMn}_2\text{O}_4/\text{Li}_4\text{Ti}_5\text{O}_{12}$ full cell based on 63 *m* WIHS (42 *m* LiTFSI + 21 *m* Pyr₁₄TFSI) delivered a stable cycle performance with over 90% capacity retention at 1 C rate (Figure 4C). Furthermore, a gel polymer electrolyte based on this 63 *m* WIHS electrolyte combined with a PAN/LiTFSI/LiOH passivation layer on the anode (details on preparation are provided in the Supporting Information) enabled the 2.5 V aqueous full Li ion cell to achieve a supreme cycle stability over 150 cycles even at 0.2 C (Figures 4D and S10) and 0.1 C (Figure S11). As reported by Dubouis et al.²⁶ hydroxides can chemically react with TFSI anions through a nucleophilic attack process and catalyze the formation of a fluorinated SEI. Such hydroxide presence should also promote the formation of LiF on the surface of $\text{Li}_4\text{Ti}_5\text{O}_{12}$ anode (Figure S12), which further suppressed H_2O reduction.

Introduction of an inert cation such as ammonium or pyrrolidinium into the WiSE electrolyte doubles the LiTFSI solubility in water and pushes the salt/water molar ratio to an unprecedented value of 1.13. The extreme salt concentration induces changes in the solvation structure around Li^+ and in the bulk electrolyte to reduce free water content and promote ion aggregation, creating a class of new aqueous electrolytes based on hybrid salt. Despite the high salt concentration of 63 *m*, the resultant electrolytes still maintain acceptable viscosity and ionic conductivity. These changes enable a wide electrochemical stability window of 3.25 V (1.75–5.0 V vs Li^+/Li) and supported the $\text{LiMn}_2\text{O}_4/\text{Li}_4\text{Ti}_5\text{O}_{12}$ full cell to deliver performances that can be hardly achieved in aqueous Li ion batteries. This work not only provides a new strategy to

design the novel aqueous electrolyte; in a broader context, the unprecedented superconcentration achieved also offers exciting new scientific opportunities in liquid structure, ion transport, and interfacial/interphasial behaviors in a region that has not been known before.

■ ASSOCIATED CONTENT

Supporting Information

The Supporting Information is available free of charge at <https://pubs.acs.org/doi/10.1021/acsenergylett.0c00348>.

Experimental section and supporting experimental data (PDF)

■ AUTHOR INFORMATION

Corresponding Authors

Oleg Borodin – *Electrochemistry Branch, Sensors and Electron Devices Directorate and Joint Center for Energy Storage Research, U.S. Army Research Laboratory, Adelphi, Maryland 20783, United States*; orcid.org/0000-0002-9428-5291; Email: oleg.a.borodin.civ@mail.mil

Kang Xu – *Electrochemistry Branch, Sensors and Electron Devices Directorate and Joint Center for Energy Storage Research, U.S. Army Research Laboratory, Adelphi, Maryland 20783, United States*; orcid.org/0000-0002-6946-8635; Email: conrad.k.xu.civ@mail.mil

Chunsheng Wang – *Department of Chemical and Biomolecular Engineering and Department of Chemistry and Biochemistry, University of Maryland, College Park, Maryland 20742, United States*; orcid.org/0000-0002-8626-6381; Email: cswang@umd.edu

Authors

Long Chen – *Department of Chemical and Biomolecular Engineering, University of Maryland, College Park, Maryland 20742, United States*

Jiaxun Zhang – *Department of Chemical and Biomolecular Engineering, University of Maryland, College Park, Maryland 20742, United States*

Qin Li – *Department of Chemical and Biomolecular Engineering, University of Maryland, College Park, Maryland 20742, United States*

Jenel Vatamanu – *Department of Chemical and Biomolecular Engineering, University of Maryland, College Park, Maryland 20742, United States*

Xiao Ji – *Department of Chemical and Biomolecular Engineering, University of Maryland, College Park, Maryland 20742, United States*

Travis P. Pollard – *Electrochemistry Branch, Sensors and Electron Devices Directorate, U.S. Army Research Laboratory, Adelphi, Maryland 20783, United States*

Chunyu Cui – *Department of Chemical and Biomolecular Engineering, University of Maryland, College Park, Maryland 20742, United States*

Singyuk Hou – *Department of Chemical and Biomolecular Engineering, University of Maryland, College Park, Maryland 20742, United States*

Ji Chen – *Department of Chemical and Biomolecular Engineering, University of Maryland, College Park, Maryland 20742, United States*; orcid.org/0000-0003-0326-8304

Chongyin Yang – *Department of Chemical and Biomolecular Engineering, University of Maryland, College Park, Maryland 20742, United States*; orcid.org/0000-0002-7127-3087

Lin Ma – Electrochemistry Branch, Sensors and Electron Devices Directorate, U.S. Army Research Laboratory, Adelphi, Maryland 20783, United States

Michael S. Ding – Electrochemistry Branch, Sensors and Electron Devices Directorate, U.S. Army Research Laboratory, Adelphi, Maryland 20783, United States; orcid.org/0000-0002-9302-1032

Mounesha Garaga – Department of Physics and Astronomy, Hunter College, City University of New York, New York, New York 10065, United States

Steve Greenbaum – Department of Physics and Astronomy, Hunter College, City University of New York, New York, New York 10065, United States

Hung-Sui Lee – Chemistry Division, Brookhaven National Laboratory, Upton, New York 11973, United States

Complete contact information is available at:

<https://pubs.acs.org/10.1021/acsenerylett.0c00348>

Author Contributions

^vL.C., J. Z., and Q. L. contributed equally to this work.

Notes

The authors declare no competing financial interest.

ACKNOWLEDGMENTS

This work was supported as part of the Joint Center for Energy Storage Research (JCESR), an Energy Innovation Hub funded by the U.S. Department of Energy, Office of Science, Basic Energy Sciences, under IAA SN2020957. L.C. and C.W. also acknowledge financial support from the U.S. Department of Energy (DOE) through ARPA-E Grant DEAR0000389. The NMR measurements conducted at Hunter College were supported in part by the Office of Naval Research (Grant N00014-16-1-2579).

REFERENCES

- (1) Armand, M.; Tarascon, J.-M. Building better batteries. *Nature* **2008**, *451*, 652–657.
- (2) Deng, J.; Bae, C.; Marcicki, J.; Masias, A.; Miller, T. Safety modelling and testing of lithium-ion batteries in electrified vehicles. *Nat. Energy* **2018**, *3*, 261–266.
- (3) Doughty, D.; Roth, E. P. A General Discussion of Li Ion Battery Safety. *Electrochem. Soc. Interface* **2012**, *21* (2), 37–44.
- (4) Balakrishnan, P. G.; Ramesh, R.; Kumar, T. P. Safety mechanisms in lithium-ion batteries. *J. Power Sources* **2006**, *155*, 401–414.
- (5) Li, W.; Dahn, J. R.; Wainwright, D. S. Rechargeable lithium batteries with aqueous electrolytes. *Science* **1994**, *264*, 1115–1118.
- (6) Luo, J. Y.; Cui, W. J.; He, P.; Xia, Y. Y. Raising the cycling stability of aqueous lithium-ion batteries by eliminating oxygen in the electrolyte. *Nat. Chem.* **2010**, *2*, 760–765.
- (7) Kim, H.; Hong, J.; Park, K.; Kim, H.; Kim, S.; Kang, K. Aqueous Rechargeable Li and Na Ion Batteries. *Chem. Rev.* **2014**, *114* (23), 11788–11827.
- (8) Suo, L.; et al. Advanced high-voltage aqueous lithium-ion battery enabled by 'water-in-bisalt' electrolyte. *Angew. Chem., Int. Ed.* **2016**, *55*, 7136–7141.
- (9) Suo, L.; Borodin, O.; Gao, T.; Olguin, T. M.; Ho, J.; Fan, X.; Luo, C.; Wang, C.; Xu, K. Water-in-salt[™] electrolyte enables high-voltage aqueous lithium-ion chemistries. *Science* **2015**, *350* (6263), 938–943.
- (10) Yamada, Y.; Usui, K.; Sodeyama, K.; Ko, S.; Tateyama, Y.; Yamada, A. Hydrate-melt electrolytes for high-energy-density aqueous batteries. *Nat. Energy* **2016**, *1*, 16129.
- (11) Yang, C.; Suo, L.; Borodin, O.; Wang, F.; Sun, W.; Gao, T.; Fan, X.; Hou, S.; Ma, Z.; Amine, K.; Xu, K.; Wang, C. Unique aqueous Li-ion/sulfur chemistry with high energy density and reversibility. *Proc. Natl. Acad. Sci. U. S. A.* **2017**, *114* (24), 6197–6202.
- (12) Yang, C.; Chen, J.; Qing, T.; Fan, X.; Sun, W.; von Cresce, A.; Ding, M. S.; Borodin, O.; Vatamanu, J.; Schroeder, M. A.; Eidson, N.; Wang, C.; Xu, K. 4.0 V Aqueous Li-Ion Batteries. *Joule* **2017**, *1*, 122–132.
- (13) Wang, F.; Borodin, O.; Gao, T.; Fan, X.; Sun, W.; Han, F.; Faraone, A.; Dura, J. A.; Xu, K.; Wang, C. Highly reversible zinc metal anode for aqueous batteries. *Nat. Mater.* **2018**, *17*, 543–549.
- (14) Yang, C.; Chen, J.; Ji, X.; Pollard, T. P.; Lü, X.; Sun, C.; Hou, S.; Liu, Q.; Liu, C.; Qing, T.; Wang, Y.; Borodin, O.; Ren, Y.; Xu, K.; Wang, C. Aqueous Li-ion battery enabled by halogen conversion–intercalation chemistry in graphite. *Nature* **2019**, *569*, 245–250.
- (15) Jiang, L.; Liu, L.; Yue, J.; Zhang, Q.; Zhou, A.; Borodin, O.; Suo, L.; Li, H.; Chen, L.; Xu, K.; Hu, Y. High-Voltage Aqueous Na-Ion Battery Enabled by Inert-Cation-Assisted Water-in-Salt Electrolyte. *Adv. Mater.* **2020**, *32*, 1904427.
- (16) Ko, S.; Yamada, Y.; Miyazaki, K.; Shimada, T.; Watanabe, E.; Tateyama, Y.; Kamiya, T.; Honda, T.; Akikusa, J.; Yamada, A. Lithium-Salt Monohydrate Melt: A Stable Electrolyte for Aqueous Lithium-Ion Batteries. *Electrochem. Commun.* **2019**, *104*, 106488.
- (17) Ding, M. S.; Xu, K. Phase Diagram, Conductivity, and Glass Transition of LiTFSI–H₂O Binary Electrolytes. *J. Phys. Chem. C* **2018**, *122*, 16624–16629.
- (18) Scatena, L.; Brown, M.; Richmond, G. Water at hydrophobic surfaces: weak hydrogen bonding and strong orientation effects. *Science* **2001**, *292*, 908–912.
- (19) Zobov, N. F.; Polyansky, O. L.; Le Sueur, C. R.; Tennyson, J. Vibration-rotation levels of water beyond the Born Oppenheimer approximation. *Chem. Phys. Lett.* **1996**, *260*, 381–387.
- (20) Eisenberg, D.; Kauzmann, W. *The Structure and Properties of Water*; Oxford University Press: London, 1969.
- (21) The dodecahedral interstitial model is described in Pauling, L. The Structure of Water. In *Hydrogen Bonding*; Hadzi, D., Thompson, H. W., Eds.; Pergamon Press Ltd: London, 1959; pp 1–6.
- (22) Borodin, O.; et al. Liquid Structure with Nano-Heterogeneity Promotes Cationic Transport in Concentrated Electrolytes. *ACS Nano* **2017**, *11*, 10462–10471.
- (23) Borodin, O.; Ren, X.; Vatamanu, J.; von Wald Cresce, A.; Knap, J.; Xu, K. Modeling Insight into Battery Electrolyte Electrochemical Stability and Interfacial Structure. *Acc. Chem. Res.* **2017**, *50*, 2886–2894.
- (24) Borodin, O.; Giffin, G. A.; Moretti, A.; Haskins, J. B.; Lawson, J. W.; Henderson, W. A.; Passerini, S. Insights into the Structure and Transport of the Lithium, Sodium, Magnesium, and Zinc Bis-(trifluoromethanesulfonyl)imide Salts in Ionic Liquids. *J. Phys. Chem. C* **2018**, *122*, 20108–20121.
- (25) Vatamanu, J.; Borodin, O. Ramifications of Water-in-Salt Interfacial Structure at Charged Electrodes for Electrolyte Electrochemical Stability. *J. Phys. Chem. Lett.* **2017**, *8*, 4362–4367.
- (26) Dubouis, N.; Lemaire, P.; Mirvaux, B.; Salager, E.; Deschamps, M.; Grimaud, A. The role of the hydrogen evolution reaction in the solid–electrolyte interphase formation mechanism for “Water-in-Salt” electrolytes. *Energy Environ. Sci.* **2018**, *11*, 3491–3499.